UC San Diego
UC San Diego Previously Published Works

Title

Integrated mutational landscape analysis of poorly differentiated high-grade neuroendocrine carcinoma of the uterine cervix.

Permalink

https://escholarship.org/uc/item/85j67132

Journal

Proceedings of the National Academy of Sciences, 121(17)

Authors

Bellone, Stefania

Jeong, Kyungjo

Halle, Mari

et al.

Publication Date

2024-04-23

DOI

10.1073/pnas.2321898121

Peer reviewed

Integrated mutational landscape analysis of poorly differentiated high-grade neuroendocrine carcinoma of the uterine cervix

Stefania Bellone[a,1], Kyungjo Jeong[b,1], Mari Kyllesø Halle[c,d], Camilla Krakstad[c,d], Blair McNamara[a], Michelle Greenman[a], Levent Mutlu[a], Cem Demirkiran[a], Tobias Max Philipp Hartwich[a], Yang Yang-Hartwich[a], Margherita Zipponi[a], Natalia Buza[e], Pei Hui[e], Francesco Raspagliesi[f], Salvatore Lopez[f,2], Biagio Paolini[f], Massimo Milione[f], Emanuele Perrone[g], Giovanni Scambia[g], Gary Altwerger[a], Antonella Ravaggi[h], Eliana Bignotti[h], Gloria S. Huang[a], Vaagn Andikyan[a], Mitchell Clark[a], Elena Ratner[a], Masoud Azodi[a], Peter E. Schwartz[a], Charles M. Quick[i], Roberto Angioli[j], Corrado Terranova[j], Samir Zaidi[k], Shuvro Nandi[l], Ludmil B. Alexandrov[l], Eric R. Siegel[m], Jungmin Choi[b,3], Joseph Schlessinger[n,3], and Alessandro D. Santin[a,3]

High-grade neuroendocrine cervical cancers (NETc) are exceedingly rare, highly aggressive tumors. We analyzed 64 NETc tumor samples by whole-exome sequencing (WES). Human papillomavirus DNA was detected in 65.6% (42/64) of the tumors. Recurrent mutations were identified in *PIK3CA*, *KMT2D/MLL2*, *K-RAS*, *ARID1A*, *NOTCH2*, and *RPL10*. The top mutated genes included *RB1*, *ARID1A*, *PTEN*, *KMT2D/MLL2*, and *WDFY3*, a gene not yet implicated in NETc. Somatic CNV analysis identified two copy number gains (3q27.1 and 19q13.12) and five copy number losses (1p36.21/5q31.3/6p 22.2/9q21.11/11p15.5). Also, gene fusions affecting the *ACLY-CRHR1* and *PVT1-MYC* genes were identified in one of the eight samples subjected to RNA sequencing. To resolve evolutionary history, multiregion WES in NETc admixed with adenocarcinoma cells was performed (i.e., mixed-NETc). Phylogenetic analysis of mixed-NETc demonstrated that adenocarcinoma and neuroendocrine elements derive from a common precursor with mutations typical of adenocarcinomas. Over one-third (22/64) of NETc demonstrated a mutator phenotype of C > T at CpG consistent with deficiencies in *MBD4*, a member of the base excision repair (BER) pathway. Mutations in the PI3K/AMPK pathways were identified in 49/64 samples. We used two patient-derived-xenografts (PDX) (i.e., NET19 and NET21) to evaluate the activity of pan-HER (afatinib), PIK3CA (copanlisib), and ATR (elimusertib) inhibitors, alone and in combination. PDXs harboring alterations in the ERBB2/PI3K/AKT/mTOR/ATR pathway were sensitive to afatinib, copanlisib, and elimusertib (*P* < 0.001 vs. controls). However, combinations of copanlisib/afatinib and copanlisib/elimusertib were significantly more effective in controlling NETc tumor growth. These findings define the genetic landscape of NETc and suggest that a large subset of these highly lethal malignancies might benefit from existing targeted therapies.

cancer | genetic analysis | oncogene | neuroendocrine | mutations

Significance

Identification of novel, effective treatment modalities for patients developing exceedingly rare, highly aggressive tumors such as high-grade neuroendocrine cervical cancer (NETc) remains an unmet medical need. Using integrated whole-exome and RNA sequencing analyses of a large set of NETc patients, we identified recurrently mutated genes and altered intracellular signaling cell pathways offering application of targeted therapies. Using two fully sequenced patient-derived xenografts harboring alterations in ERBB2/PIK3CA/AKT pathways, we found copanlisib (PIK3CAi), afatinib (pan-HERi), and elimusertib (ATRi) monotherapy as well as the combination of copanlisib/afatinib and copanlisib/elimusertib to significantly inhibit NETc PDXs growth. Our integrated genetic analysis combined with in vivo preclinical validation experiments suggests that a large subset of high-grade NETc may potentially benefit from the repurposing of targeted drugs.

[1]S.B. and K.J. contributed equally to this work.

[2]Present address: Gynecologic Oncology Unit, Istituti di Ricovero e Cura a Carattere Scientifico (IRCCS) Istituto Tumori Giovanni Paolo II, 70124 Bari, Italy.

[3]To whom correspondence may be addressed. Email: jungminchoi@korea.ac.kr, joseph.schlessinger@yale.edu, or alessandro.santin@yale.edu.

High-grade, poorly differentiated neuroendocrine cancer of the uterine cervix (NETc) is an exceedingly rare tumor (0.9 to 1.5% of all cervical malignancies) associated with an extremely poor prognosis as a result to its propensity for early spread to lymphatics and distant metastasis (1, 2). Due to its rarity, there has been no prospective clinical study developing standard treatment algorithms specific for NETc patients. For early-stage disease, patients typically undergo radical surgery, similar to the treatment given to cervical cancer patients with the most common histology, such as squamous, adenosquamous, and adenocarcinoma. For advanced-stage disease, chemoradiation is the standard approach. Meanwhile, patients with metastatic disease often receive palliative systemic chemotherapy, using regimens common for small cell lung cancer (i.e., microcitoma), like cisplatin and/ or carboplatin combined with etoposide. However, outcomes remain poor with a median survival for NETc patients of less than 2 y compared with a median survival of over 10 y for patients with squamous tumors (3). A deeper understanding of the molecular basis of NETc and the development of novel effective treatments remain an unmet medical need.

A small number of studies, most of which either used limited next-generation sequencing (NGS) platforms or reported comprehensive data from just a handful of tumor samples, have recently evaluated the genetic landscape of NETc (4–8). In this report, we analyzed a large set of high-grade NETc tumor samples (66 tumor specimens from 64 patients) available through a multi-institutional study collaboration between Yale University and other academic sites in the United States, Italy, and Norway. We used whole-exome (WES) and RNA sequencing (RNA-Seq) to perform an integrated genetic analysis of a cohort of NETc, which included two patient-derived xenografts (PDXs). A subset of these samples included multiregion WES of samples demonstrating neuroendocrine tumor cells admixed with epithelial (i.e., glandular) adenocarcinoma cells (herein, labeled as mixed NETc). Our results

revealed that multiple genes harbor recurrent mutations and increased numbers of somatic single-nucleotide (SNV) and copy number variations (CNV), a dominant methylcytosine-binding domain (MBD4) deficiency signature and clinically actionable pathways including the mismatched repair (MMR) and PTEN/ERBB2/PI3K/AKT/mTOR pathways active in a large number of NETc. Tumors with mixed adenocarcinoma and NETc histology demonstrated that NET elements derive from the clonal metaplastic transformation of a common precursor having mutations typical of carcinomas. Finally, the establishment of NETc patient-derived xenografts (PDXs) harboring alterations in the ERBB2/PI3K/AKT/mTOR pathways enabled in vivo assessment of potential drug responses to multiple inhibitors including i) pan-HERi (i.e., afatinib); ii) PIK3CAi (i.e., copanlisib); and iii) ATRi (i.e., elimusertib). We found the activity of these inhibitors in both NETc xenografts with significantly longer tumor regression when exposed in vivo to combinations of pan-HER/PIK3CA and PIK3CA/ATR inhibitors compared with single agents. Our integrated analysis results define a set of mutated genes and pathways involved in high-grade NETc carcinogenesis and provide a strong preclinical rationale for clinical trials targeting specific driver mutations/pathways in patients with advanced/metastatic or recurrent NETc.

Results

Cohort Characteristics. We analyzed the sequencing data of 66 NETc from 64 patients, including 57 samples with matched normal DNA and seven unmatched tumors. A total of 105 samples were sequenced after DNA extraction from FFPE tissues while 20 were from fresh samples. NET samples were obtained from patients harboring stage I (30/64 = 47%), stage II (10/64 = 16%), stage III (12/64 = 19%), and stage IV (12/64 = 19%) disease (*SI Appendix*, Fig. S1). The clinical and histological features are summarized in *SI Appendix*, Table S1. Among the 64 included patients, WES and RNA-Seq were performed on 66 and eight tumor samples, respectively.

Genetic Landscape of NETc. Tumor and normal samples displayed a mean coverage of 179.6 and 88.2 independent sequencing reads per targeted base, respectively (*SI Appendix*, Table S2). Average tumor purity was 53.3% and showed no correlation with somatic mutation burden (R^2 = 0.016, P = 0.95). A total of 28,918 somatic variants (median = 156.00; range 7 to ~3,113) were detected, including 27,011 single-nucleotide variants (SNVs) and 1,076 small insertions and deletions. Tumor mutation burden in NET compared with squamous and adenocarcinoma cervical cancer histology (9) showed

that the average nonsilent mutation rate across NETc was 9.81/Mb with a median of 3.47/Mb, significantly higher than cervical adenocarcinoma (ACA: mean = 2.91/Mb, median = 1.82/Mb) based on the Wilcoxon test (P = 0.040). However, no significant differences were identified between NET and cervical cancer with squamous histology (SCC: mean = 5.01/Mb, median = 4.53/Mb) (P = 0.875) (9). Human papillomavirus (HPV) DNA was detected in 42 of the 64 (66%) tumor samples (*SI Appendix*, Fig. S2). HPV integration within the 8q24 region was identified in 12 samples (19%). This region includes the c-MYC oncogene, a previously reported HPV-integration site hotspot (10). No significant difference in median overall survival (OS) was noted between the two cohorts of HPV+ and HPV- NETc (HPV+, 45 mo vs. HPV–, 54 mo, P = 0.629, log-rank test). Using the published Alexandrov's genetic signature algorithm (11), we identified 22 NETc (34%) harboring a rare mutator phenotype of C > T at CpG consistent with deficiencies in the function of *MBD4* (*SI Appendix*, Fig. S3). This gene encodes a methylcytosine-binding domain (MBD)-containing a base excision-repair (BER) glycosylase that prevents mutability at CpG sites that, when inherited as a germline mutation, causes a multitumor predisposition syndrome (12). Since *MBD4* deficiency in a subset of human tumors has been recently associated with hypermutation and clinical responses to immune checkpoint inhibitors (ICI) (13, 14) we compared the tumor mutation burden (TMB) of the "MBD4"-like group vs. the remaining NETc after excluding six samples harboring genetic signatures consistent with mismatch-repair (MMR) deficiency (i.e., signatures SBS6, SBS20, and SBS26). NETc samples harboring the MBD4 signatures demonstrated a significantly higher TMB when compared to the remaining NETc (Welch's t test; P = 0.001). The remaining samples harbored signatures consistent with SBS1 (aging), SBS2 (APOBEC), SBS5 (aging), SBS13 (APOBEC), and SBS18 (ROS) with a single sample (1.5%) presenting an SBS3 mutational signature previously reported to correlate with BRCA1 and BRCA2 biallelic inactivation and homologous recombination defect (HRD) (*SI Appendix*, Fig. S4) (11).

Analysis of Single-Nucleotide Variants. Somatic mutational analysis results of 64 tumors are shown in Fig. 1 and *SI Appendix*, Table S3. Recurrent somatic mutations were detected in multiple genes including *PIK3CA, K-RAS, NOTCH2, KMT2D/MLL2, PTEN, RB1, JAK1, CREBBP, RPL10, MIA2, FAM124A, ELOA2,* and *ZNF788P* (*SI Appendix*, Table S3). Mutations in the *PIK3CA* gene included the hotspot E542K and E545K sites (8%, 5/64 samples) located in the catalytic subunit of phosphoinositide-3 kinase, K-RAS hotspot mutations at G12D (3%, 2/64 samples), missense mutations in *KMT2D/MLL2*, a methyltransferase gene
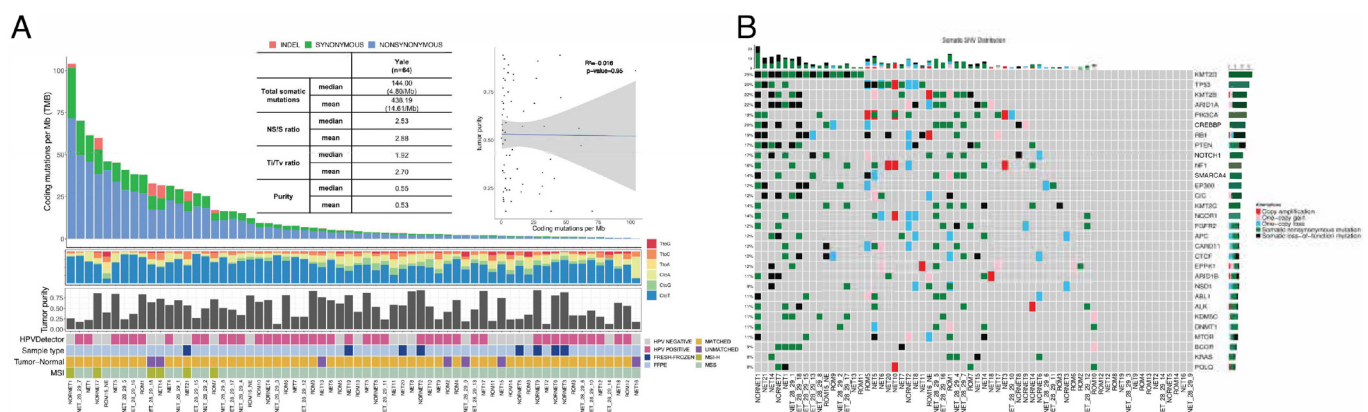

Fig. 1. Somatic mutation landscape underlying NETc. (*A*) Distribution of somatic mutation in 64 NETc samples. (*B*) Frequency and type of somatic mutations. Rows represent genes affected by at least two somatic SNVs or small INDELs, and columns represent individual NETc.

with chromatin remodeling activities, at p.P4916L, and a mutation in *RPL10* (K133R, 3/64 samples). This gene encodes for an essential protein near the ribosomal catalytic core. Similarly to the better characterized R98S *RPL10* mutation, this recurrent mutation may potentially disrupt ribosome function and cell proliferation (15). Recurrent mutations also occurred in *ZNF788P* (*SI Appendix*, Table S3), a pseudogene encoding for a zinc finger protein involved in various aspects of transcriptional regulation (16); *NOTCH2*, a gene previously reported to function as a regulator of neuroendocrine differentiation (17); *ARID1A*, the DNA-binding subunit of the SWI/SNF (switch/sucrose nonfermentable) chromatin remodeling complex, which regulates a wide range of cellular processes, including transcription, replication and DNA damage repair (18); and the melanoma inhibitory activity 2 (*MIA2*) gene, which has previously been associated with lymph node metastasis and inhibition of apoptosis in oral squamous carcinoma. Importantly, increased levels of expression of the MIA2 gene have been reported during the progression from high-grade cervical intraneoplasia-3 (CIN3) to invasive cervical cancer (19).

WDFY3 Identified As a Driver of NETc. To identify genes with an increased burden of somatic mutation, we analyzed the burden of all protein-altering somatic mutations. We identified five significantly mutated genes with a genome-wide false discovery rate (FDR) of 0.05 (Fig. 2*A* and *SI Appendix*, Table S4). While alterations in *RB1* (13%, FDR = 2.20×10^{-5}), *ARID1A* (17%, FDR = 1.69×10^{-4}), *KMT2D*, (25%, FDR = 3.31×10^{-2}), and *PTEN* (16%, FDR = 3.76×10^{-2}) (4–8) have previously been reported in NETc, WD Repeat, and FYVE Domain Containing 3 (*WDFY3*) gene mutations have not previously been described and occurred in 14% of patients (FDR = 3.79×10^{-2}) (Fig. 2*B*). *WDFY3* encodes a phosphatidylinositol 3-phosphate-binding protein that functions as a master conductor for aggregate clearance by autophagy. This protein shuttles from the nuclear membrane to colocalize with aggregated proteins, where it complexes with other autophagic components to achieve macroautophagy-mediated clearance of these aggregated proteins (20, 21). Autophagy is under the control of class I PI3K/AKT/mTOR and AMPK signaling pathways (20, 21). Of interest, 14 out of 17 of the *WDFY3* carriers had overlapped alterations of PI3K and AMPK pathways (Fig. 2*C*), suggesting these genetic alterations and pathways may work together to drive NETc tumorigenesis. After manual visual inspection, CNV losses in WDFY3 were detected in eight additional patients, accounting for 12.5% of the total cohort. To confirm that these were loss-of-function events, we analyzed RNA-Seq data on these patients, along with 3 noncarriers. Patients with *WDFY3* alterations showed lower mean expression values (7,095.47 vs. 12,338.24 normalized counts), although the difference was not statistically significant (*SI Appendix*, Fig. S5, P_{adj} = 0.78, negative binomial test). Furthermore, alterations of *WDFY3* were rarely found in neuroendocrine tumors (NETs) from other organs such as lungs, pancreatic, and prostate (2.7%) or human solid tumors from The Cancer Genome Atlas (4.9%), supporting the notion of a role in NET tumorigenesis. These results provide evidence for a link between *WDFY3* alterations and cervical NET.

Copy Number Variation in NETc. We next assessed somatic CNVs in 57 matched tumors. Statistically significant focal amplified regions and deleted regions were detected using GISTIC2.0 (10). Chromosome 3q27.1 (chr3:176763997 to 189456599) including the oncogenes *PIK3CA, ELF4A2*, and *TBL1XR1* was amplified in 5 (9%) of the tumors (Fig. 3). *TBL1XR1* has previously been reported to be amplified in neuroendocrine disease. Furthermore, several oncogenes that co-occur with gains in the 3q26-27 region, including *ATR/PI3K*-involved genes and *BCL6*, can be therapeutically targeted in cancer (22). Also, 19q13.12 (chr19:33439201 to 36831999) amplification was identified in 7 (12%) of the samples, the interval of which includes *CEBPA*. *CEBPA* is well known as a master regulator of various oncogenic processes like cell cycle regulation, proliferation, and angiogenesis (23). Despite not being statistically significant, focal peak gains or amplifications were found in 25 patients (44%) in the 19q12 region, including *CCNE1*, which is located nearby. Chromosome 1p36.21 (chr1:1 to 21,083,785) was deleted in 3 (5%), 5q31.3 (chr5:140,031,401 to 140,890,399) in 4 (7%), 6p22.2 (chr6:25,983,442 to 27,425,184) in 2 (4%), 9q21.11 (chr9:35,680,801 to 71,661,360) in 5 (9%), and 11p15.5 (chr11:1 to 1,491,432) in two samples (4%) (FDR < 0.25, Benjamini–Hochberg correction) (Fig. 3). Tumor-suppressor genes were identified at the 1p36.21 and 9q21.11 including *RPL22, SDHB, TNFRSF14, SPEN, CAMTA1,* and 9q21.11 (*PAX5*). Among identified tumor-suppressor genes, *PAX5* acts as

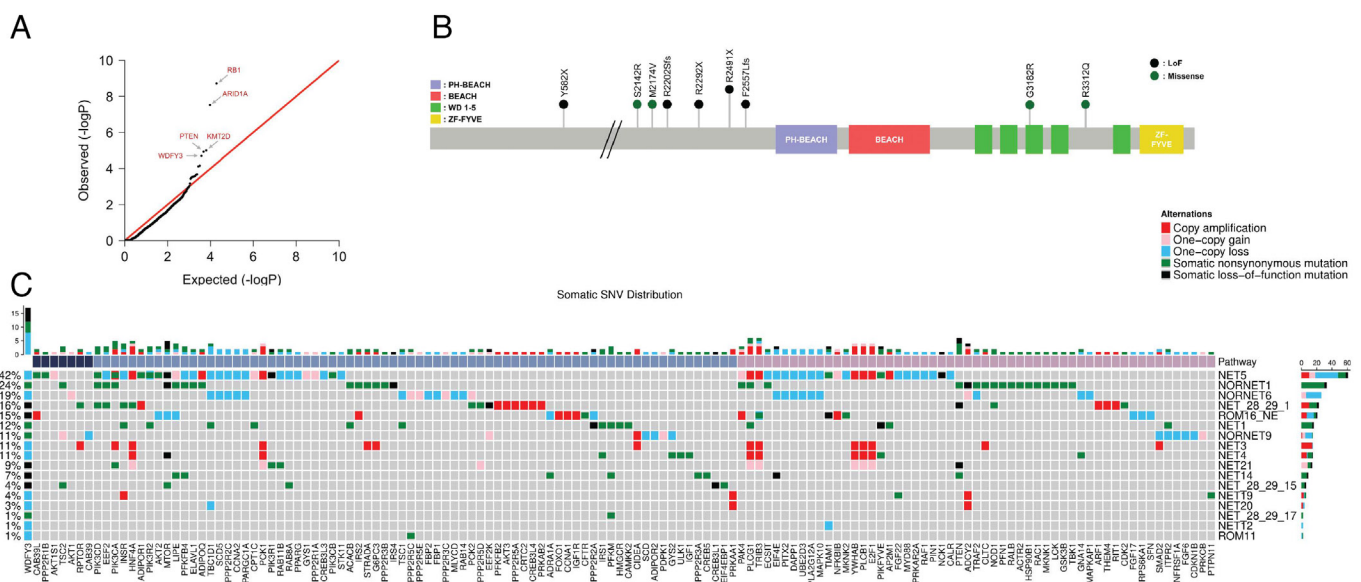**Fig. 2.** Mutational gene burden in NETc. (*A*) Q-Q plot of significantly mutated genes according to Mutpanning including *RB1, ARID1A, KMT2D, PTEN,* and *WDFY3*. (*B*) Representation of SNVs and INDELs detected in the *WDFY3* gene. (*C*) Frequency and type of PI3K and AMPK somatic mutations in samples harboring *WDFY3* gene alterations. Pathway: PI3K/AMPK (deep navy), PI3K (light pink), and AMPK (light navy).
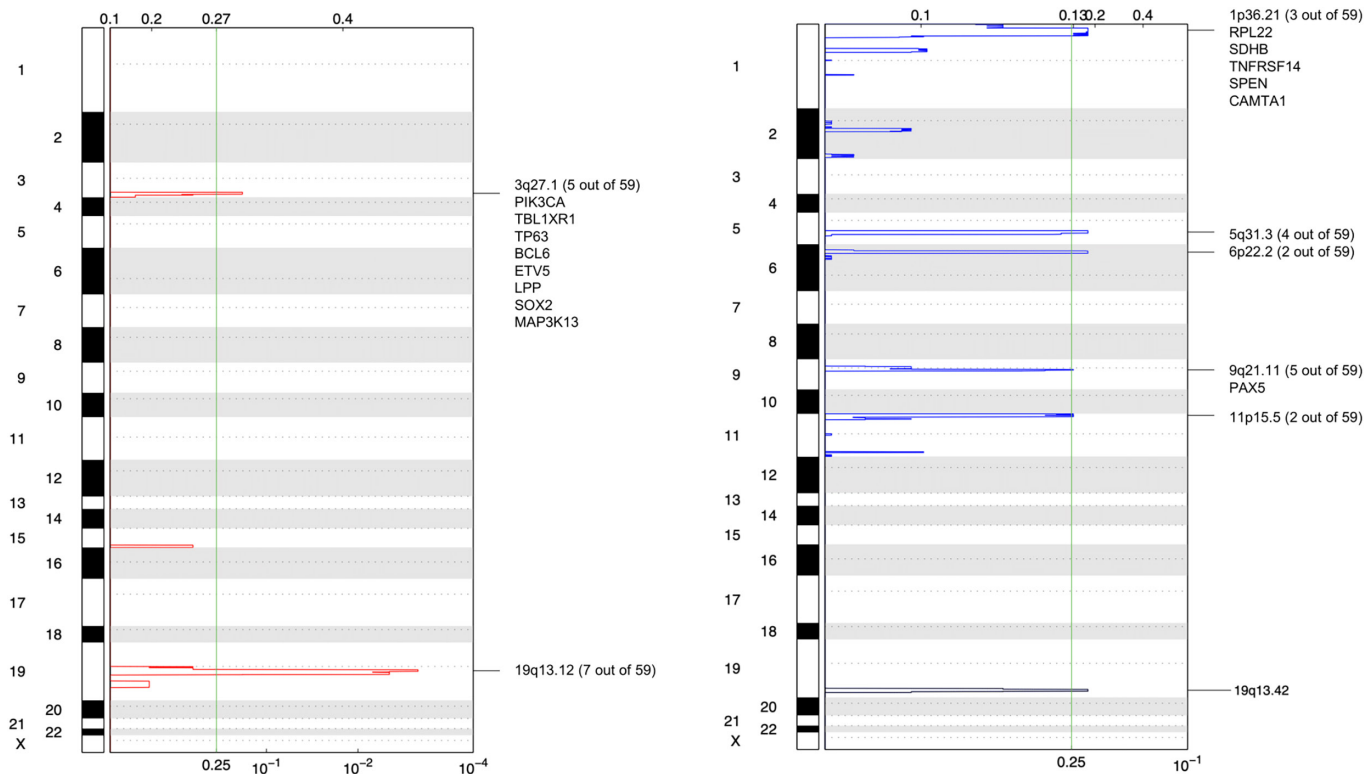
Fig. 3. Recurrent CNV pattern. Significant amplifications (*Left*) and deletions (*Right*). The green line indicates the cutoff for significance (q = 0.25). In the deletion result, the black peak indicates the false positive by visual inspection.

a positive regulator of c-Met transcription and has been suggested as a therapeutic target in small cell lung cancer (24).

Gene Fusion Analysis. Eight NETc samples were subjected to RNA-Seq and analyzed for gene fusion events as described in *Materials and Methods*. We found one of the eight NETc samples (i.e., NORNET2) to harbor two confirmed fusion events (i.e., ACLY-CRHR1 and PVT1-MYC). As depicted in *SI Appendix,* Fig. S6, the ACLY-CRHR1 gene fusion caused upregulation of CRHR1 in the NORNET2 sample. Similarly, as described in *SI Appendix,* Fig. S7, the PVT1-MYC gene fusion also caused upregulation of the MYC gene in the NORNET2 tumor sample.

Evolution and Clonal Relationship of NET Admixed with Adenocarcinoma Cells. To determine whether the adenocarcinoma and neuroendocrine components in the mixed cervical NETs arise independently as two histologically distinct synchronous tumors or represent the product of metaplastic transformation of one histology into the other, we performed a clonal evolution analysis of two mixed NETc samples (i.e., ROM15 and ROM16) where each histology was macrodissected before sequencing. We identified a total of 1,877 somatic mutations in ROM15, 720 in the adenocarcinoma component and 1,034 in the neuroendocrine component, while ROM16 demonstrated a total of 616 somatic mutations, 202 in the adenocarcinoma component and 340 in the neuroendocrine component (Fig. 4A). The ROM15 sample shared 123 (6.6%) somatic mutations including *ACVR1B, STAG2,* and *BAP1* between the adenocarcinoma and the neuroendocrine components, while the ROM16 sample shared 74 (12.0%) of somatic mutations including *ATM, ERBB4* and *NSD1* between the two components. When the clonal architecture cancer cell fractions adjusted for tumor purity were clustered using PyClone (25) and the phylogenetic trees were reconstructed using ClonEvol (26), a branching structure was revealed, demonstrating that both mixed NETc specimens shared a

common adenocarcinoma ancestry before clonally evolving in the neuroendocrine components (Fig. 4B). Neuroendocrine tumors from ROM15 and ROM16 carried a notable missense mutation in *NOTCH1* which is consistent with previous reports linking NOTCH1 signaling to regulation of neuroendocrine differentiation (*SI Appendix,* Table S5). Overrepresentation analysis (ORA) displayed significant enrichment of NETc-specific mutated genes from 64 samples in the NOTCH signaling pathway (*SI Appendix,* Table S6). Of interest, while examining the altered genes of the neuroendocrine tumor, terms related to Rho GTPase from the Reactome database were statistically significant: Rho GTPase Cycle (P_{adj} = 9.27E-10) and Signaling by Rho GTPase (P_{adj} = 2.68E–05) (*SI Appendix,* Table S6), suggesting that Rho GTPases may also play an important role in neuroendocrine differentiation. This association was not significant for mutated genes in adenocarcinoma (P_{adj} = 0.17 and 0.23). Importantly, mutations in 36 canonical Rho GTPase, GEF, and GAP gene set were found at significantly higher rates in ROM15/16 NETc than in ROM15/16 adenocarcinomas, as shown in *SI Appendix,* Table S7 (binomial test, P = 0.02).

Pan-HER, PIK3CA, and ATR Inhibitors Are Active In Vivo against NETc PDXs. Since 57.8% (37 out of 64) of the NETc patients harbored alterations in the PTEN/PIK3CA/AKT/mTOR pathway (*SI Appendix,* Fig. S8), 64.1% (41 out of 64) demonstrated alterations in the AMPK pathways (*SI Appendix,* Fig. S9), and 14.1% (9 out of 64) displayed amplification in the ERBB signaling pathway, with 6 out 64 in ERBB2 and 4 out of 64 in ERBB3 (*SI Appendix,* Fig. S10), we utilized two recently established NETc PDX (i.e., NET19 and NET21) harboring hot spot mutations (p.E542K and p.E545K) in *PIK3CA* and loss of function in *PTEN* (i.e., NET21, *SI Appendix,* Figs. S8, S9, and S11) and/or copy gain of c-*ERBB2* and *ERBB3* genes (i.e., NET19, *SI Appendix,* Fig. S11) to evaluate the activity of three small molecule inhibitors namely 1) elimusertib (BAY 1895344, Bayer Pharmaceuticals Inc.), an ATRi currently in Phase II clinical
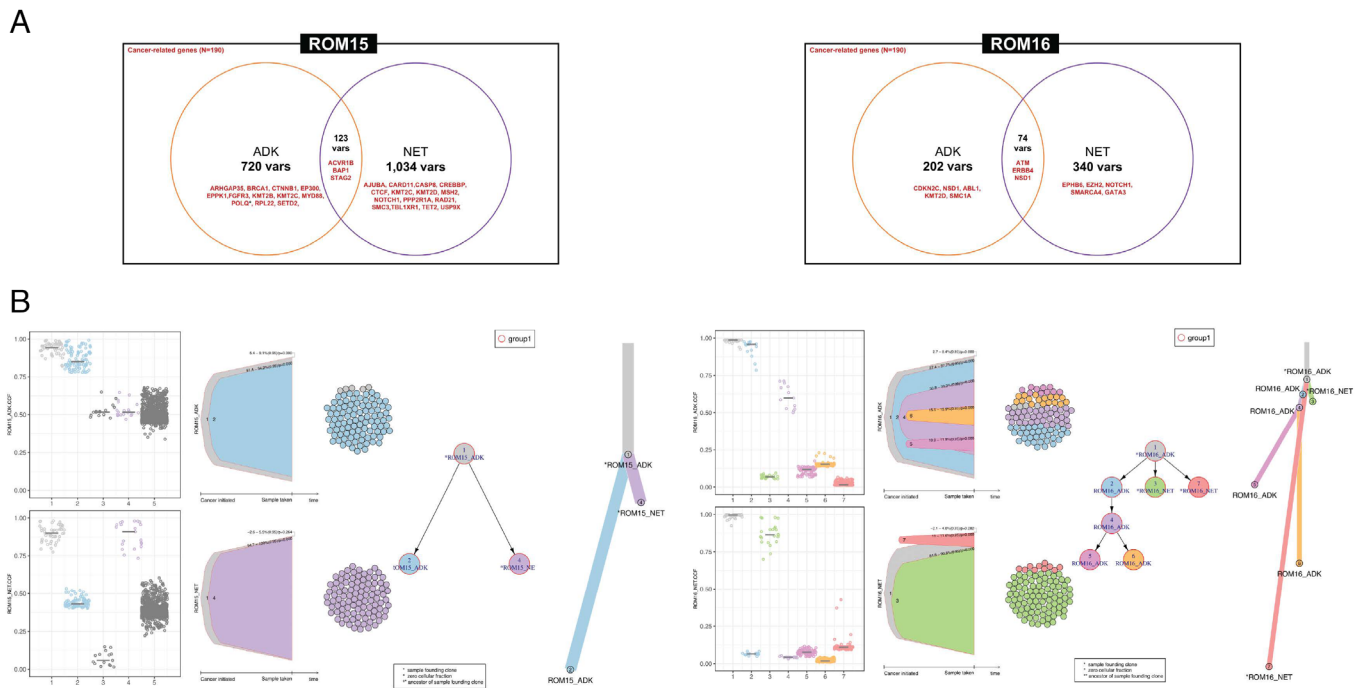
Fig. 4. (*A*) Genomic comparison of neuroendocrine and adenocarcinoma cells and evolution paths of two mixed NETc samples. Venn diagrams present the total number of somatic exonic mutations unique to neuroendocrine (NET) vs. epithelial (ADK) cells or shared between the ROM15 and ROM16 matched mixed tumors. (*B*) Clustering of subclones and clonal evolution inference in the mixed ROM15 and ROM16 NETc. *Left*: Clusters of variants based on the variant allele fraction (VAF) in neuroendocrine and epithelial cells. Points represent the VAFs of each variant in each cluster. *Middle*: Node-based clonal evolution trees. *Right*: Branch-based clonal evolution trees. Branch lengths represent the number of somatic variants in the clusters.

trials against multiple solid human tumors, 2) copanlisib (Bayer Pharmaceuticals Inc.), an intravenous, selective pan-Class I PI3K inhibitor highly active in PIK3CA mutant tumors approved by the Food and Drug Administration (FDA) for the treatment of patients with relapsed follicular lymphoma, and 3) afatinib (Boehringer Ingelheim Inc.), a pan-c-ERBi approved for use in EGFR mutated lung cancer patients. We found single-agent afatinib, copanlisib and elimusertib to significantly inhibit tumor growth when compared to vehicle-treated mice in both PDX NETc models. Indeed, as shown in Fig. 5*A* for the NET19 PDX, mice receiving copanlisib (5 mg/kg QD) or afatinib (7.5 mg/kg BID) demonstrated a significantly slower tumor growth rate compared to vehicle control (Fig. 5*A*, $P < 0.0001$ and $P < 0.0001$, respectively). Similarly, NET21 PDX mice treated with a twice-daily oral treatment with elimusertib (20 mg/kg) or copanlisib (5 mg/kg QD) exhibited a significantly slower tumor growth rate compared to vehicle control (Fig. 5*B*, $P = 0.0008$ and $P = 0.007$, respectively). Importantly, the combinations of the two inhibitors afatinib and copanlisib in NET19 and elimusertib and copanlisib in NET21 induced a more durable tumor growth inhibition in both PDX models when compared to single agent treatment (Fig. 5 *A* and *B*, $P = 0056$ and $P = 0.0004$, and $P = 0.009$ and $P = 0.0004$, respectively), with no evidence of increased acute or chronic toxicity in the animals (data not shown).

Discussion

Poorly differentiated, high-grade neuroendocrine carcinomas of the uterine cervix are extremely rare, highly lethal tumors that disproportionately affect young women (1–3). We report the whole-exome sequencing analysis of the largest cohort of high-grade cervical NET to date. Importantly, multiregion sequencing of NET samples harboring both neuroendocrine and adenocarcinoma cells (i.e., mixed NETc) provided us with the opportunity to resolve the evolutionary history of NETc. Just as importantly, the availability and comprehensive WES characterization of two NETc PDXs allowed us to

preclinically evaluate whether specific mutation profiles and/or derangement in the PTEN/PIK3CA/AKT/mTOR genes and AMPK pathways may be "druggable" in NETc patients. Accordingly, our integrated results define the genetic hallmarks of this difficult-to-treat variant of cervical carcinoma and identify multiple mutated genes and deranged pathways potentially targetable with currently available therapeutic drugs.

The number and type of somatic mutations (i.e., mutational signatures) extracted from WES may vary widely between cancer types even within the same organ since they are the consequence of multiple mutational processes. In our NETc series, the total coding mutational burden was higher when compared to cervical adenocarcinomas but not significantly different from that found in squamous cervical tumors (9). Similarly to the more common squamous and adenocarcinoma histology, we found most NETc to harbor high-risk HPV genotypes. Of interest, a substantial fraction (i.e., over one-third) of the NETc demonstrated a genetic signature associated with deficiencies in *MBD4*, a gene encoding a methylcytosine-binding domain (MBD) glycosylase that prevents mutability at CpG sites. This pattern has previously been observed in patients harboring deficiency in the base excision repair (BER) pathway secondary to rare biallelic loss-of-function germline variants of *MBD4* (12). In that study, the genetic signature identified a group of patients characterized by a multiorgan tumor predisposition syndrome, including adenomatous colorectal polyposis, acute myeloid leukemia, and uveal melanoma (12). Importantly, *MBD4* has previously been reported to represent a binding partner of the mismatch repair (MMR) protein MLH1, enabling modulation of the levels of core MMR proteins (27) and causing hypermutation (13, 14). Consistent with these studies, the tumor mutation burden (TMB) of the "MBD4"-like NETc group was significantly higher when compared to the remaining NETc samples (Welch's *t* test; t = 3.622, $P = 0.0001$). However, with the single exception of a NETc sample harboring a mixed of MSI-H/MBD4 signature (i.e., NORNET1), none of the remaining 22 samples harboring a mutator phenotype of C > T at CpG
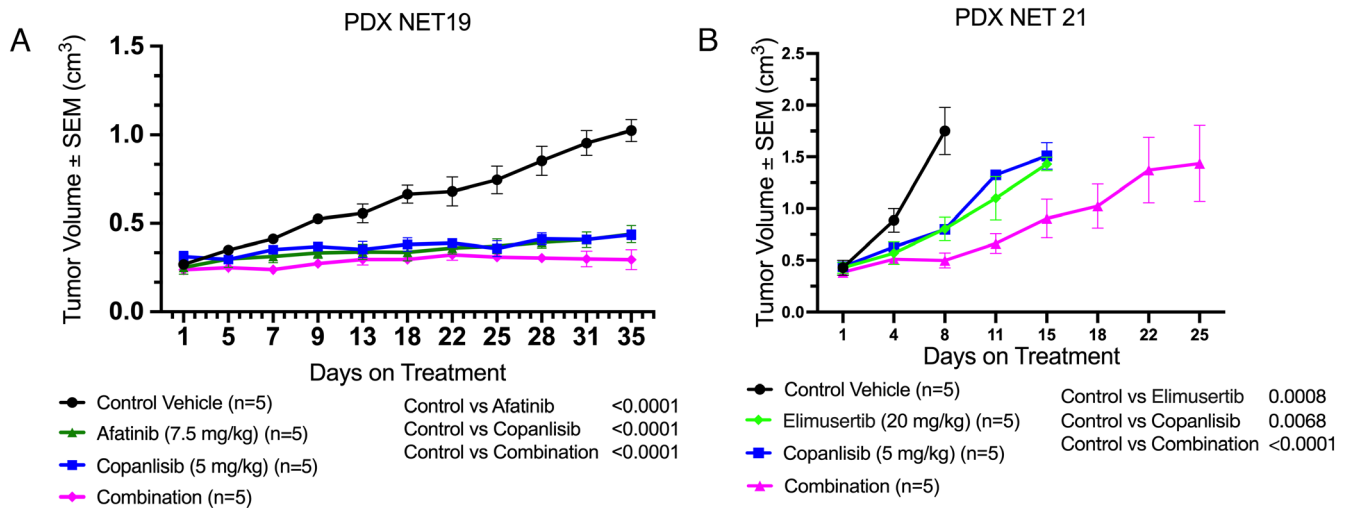
Fig. 5. Copanlisib, afatinib, and elimusertib alone or in combination inhibited cell proliferation in NET19 and NET21 PDXs. (*A*) Mice harboring NET19 PDX were treated with vehicle, copanlisib and afatinib or the combination of the two up to 30 d. Tumor volumes are reported as mean ± SEM. Tumor growth was significantly different between control and mice treated with copanlisib, afatinib, or the combination of copanlisib and afatinib (Fig. 5*A*, $P < 0.0001$, $P < 0.0001$, and $P < 0.0001$, respectively). The combinations of the two inhibitors induced a more durable tumor growth inhibition in the NET19 PDX model when compared to either copanlisib or afatinib alone (Fig. 5*A*, $P = 0.0004$ and $P = 0.0056$, respectively) (*B*) Mice harboring NET21 PDX were treated with vehicle, copanlisib and elimusertib or the combination of the two up to 30 d. Tumor volumes are reported as mean ± SEM. Tumor growth was significantly different between control and mice treated with copanlisib or elimusertib or the combination of copanlisib and elimusertib (Fig. 5*B*, $P = 0.007$, $P = 0.0008$, and $P < 0.0001$, respectively). While the combination of the two inhibitors was not able to induce a durable treatment response in this tumor model, it significantly slowed down tumor growth when compared to copanlisib and elimusertib alone (Fig. 5*B*, $P = 0.0004$ and $P = 0.009$, respectively).

consistent with deficiencies in the function of *MBD4*, demonstrated hyper- or ultramutation characteristics consistent with MMR and/or POLE/POLD deficiency. Taken together these findings demonstrate a higher TMB in NETc samples harboring an *MBD4* signature and suggest that this subset, similarly to other *MBD4* deficient human tumors originating from other organs (12–14) may be sensitive to immune checkpoint inhibitor (ICI) treatment. Consistent with this hypothesis, two case reports have recently described exceptional responses to immune checkpoint (anti-PD-1) immunotherapy in NETc patients (28, 29).

Multiple recurrent mutations in well-recognized cancer genes, including the "driver" hotspot SNV p.E542K and pE545K mutations in *PIK3CA*, part of the ERBB2/PI3K/AKT/mTOR pathway, were identified by WES. *RB1, PTEN, KMT2D/MLL2,* and *ARID1A* mutations were also identified in a significant subset of NETc. These results corroborate those of other studies reporting on the genetic landscape of NETc (4–8) and support the notion that inactivation of these well-established tumor suppressor genes or gain of function in well-characterized oncogenes plays an important role in NETc carcinogenesis. Of interest, 14% of the NETc demonstrated SNV alterations in *WDFY3* with an additional 12.5% demonstrating by CNV a loss of function of *WDFY3*. This gene encodes for a clinically relevant macroautophagic scaffold protein that is linked to mitophagy/autophagy, neurodevelopment, intellectual disability, and autism spectrum disorder (15). Fourteen out of 17 WDFY3 carriers also had overlapped alterations in the PI3K and AMPK pathways. Since autophagy is known to be regulated through the PI3K/AKT/mTOR and AMPK signaling pathways, it is likely that these genetic alterations may work in combination as drivers of NETc tumorigenesis. Finally, NETc harboring *WDFY3A* alterations also demonstrated a significantly higher TMB (FDR = 0.0379).

Using CNV analysis we identified two somatic CNV-gains that occurred more often than expected by chance on chromosome 3 and 19. Notably, six NETc also had focal gains/amplifications of the segment of chromosome 8 containing c-MYC, while 25 (44%) demonstrated focal gain/amplifications in CCNE1 on Chr 19, confirmed by visualization based on coverage. CCNE1 is known to play a significant role in cell proliferation, differentiation, and transcriptional

regulation in multiple human tumors. Importantly, bromodomain and Extra-Terminal motif (BET) and CCNE1 inhibitors have already demonstrated preclinical activity in human tumors harboring c-MYC and CCNE1 gain of function mutations (30, 31) and are currently in clinical trials, suggesting they may represent additional therapeutic tools to effectively target a subset of recurrent, chemotherapy-resistant NETc.

High-grade neuroendocrine tumors include both the small cell carcinoma and large cell carcinoma phenotypes. However, in some NETc patients, mixed tumors containing both adenocarcinoma (AC) and neuroendocrine cells are identified (*SI Appendix*, Table S1). In these patients the clinical behavior of mixed types of NETc is determined by the neuroendocrine component and, accordingly, these tumors are classified and managed as pure NETc (32). However, the origin and relationship of the admixed populations of phenotypically different tumor cells in NETc have not been established. Accordingly, in this study, we used macrodissection and multiregion sequencing of neuroendocrine vs. adenocarcinoma areas of two mixed NETc to perform a clonal evolution analysis of the samples. Our results demonstrate that the adenocarcinoma and neuroendocrine elements share many somatic mutations, establishing unequivocally the common genetic origin of these tumors. Our finding demonstrating that the root mutations include mutations well-established to play a role in cervical adenocarcinomas is consistent with an epithelial origin of NETc.

The HER2/neu/phosphatidylinositol 3-kinase/AKT (PI3K/AKT)-mammalian target of rapamycin (mTOR) signaling cascade plays a central role in diverse cellular responses such as proliferation, survival, mobility, metabolism, and control of malignant cellular growth (33). Our WES results demonstrated that 58% (37 out of 64) of the NETc patients harbored alterations in the PTEN/PIK3CA/AKT/mTOR pathway while 64% (41 out of 64) demonstrated derangements in the AMPK pathway (*SI Appendix*, Figs. S8 and S9). Given that a large number of NETc may be addicted to these genetic alterations, we took advantage of two recently established and fully sequenced PDXs harboring derangement in these pathways to evaluate whether such alterations are predictive of drug response to i) afatinib (i.e., a pan-HERi); ii) copanlisib (i.e., a PIK3CAi);

and iii) Elimusertib (i.e., a ATRi). We found single-agent copanlisib, afatinib and elimusertib to have a significant but limited activity against *PIK3CA* mutated cell lines in vivo, and accordingly, single agents were only transiently effective in vivo in controlling the growth of NET19 and NET21 xenografts. Importantly, the combination treatments of copanlisib/afatinib in NET19 and copanlisib/elimusertib in NET21 were significantly more effective, inducing longer regression of NETc tumors harboring derangements in the PI3K/AKT/mTOR pathway. Taken together, these results suggest that a large subset of NETc might greatly benefit from existing ERBB2/PIK3CA/AKT/mTOR targeted drugs.

Finally, to identify putative gene fusions, we analyzed transcriptomic data from 8 NETc fresh samples. We found two fusion events (i.e., ACLY-CRHR1 and PVT1-MYC). The first gene fusion caused upregulation of the CRHR1 gene in the NETc sample, NORNET2. CRHR1 encodes a G-protein coupled receptor that binds neuropeptides of the corticotropin-releasing hormone family that are major regulators of the hypothalamic–pituitary–adrenal pathway. The encoded protein is essential for the activation of signal transduction pathways that regulate diverse physiological processes including stress, reproduction, immune response, and obesity (34). The other gene fusion, PVT1-MYC, caused upregulation of the MYC gene in the same patient. PVT1 is widely recognized for its interaction with MYC, an oncogene identified as a driver of cell proliferation in multiple human tumors (35). Further efforts will be required to determine the impact of CRHR1 alterations in NETc.

In conclusion, our integrated whole-exome and RNA-Seq results defined the genetic landscape of NETc and identified multiple potentially actionable deranged genes/pathways. Since advanced/recurrent and/or metastatic NETc remain incurable, our comprehensive genetic results, combined with preclinical validation data using NETc PDX models strongly suggest that the ERBB2/PI3K/AKT/mTOR deranged pathway and high number of mutations detected in NETc with MBD4 and MSI-H signatures may be clinically susceptible to targeted inhibitors or immune checkpoint inhibitors, respectively. These findings will help guide further research and targeted therapies against this highly lethal cancer worldwide.

Materials and Methods

Patient and Specimen Acquisition. The study protocol was approved by the Yale Human Investigation Committee. Prior to surgical staging and/or biopsy, patients were consented for tumor banking in accordance with the Declaration of Helsinki. DNA (105 samples from formalin-fixed paraffin-embedded tissues) and/or RNA (total of 20 fresh-frozen samples) with matched normal tissue from 57 patients were extracted from a total 64 NETc patients including two PDXs, who underwent staging/treatment at Yale University, New Haven, CT, the University of Brescia School of Medicine, Brescia, Italy, the University of Bergen (UoB), Bergen, Norway, the Istituto Nazionale dei Tumori di Milano, Milan, Italy, the Policlinico Universitario A. Gemelli, Rome, Italy, the University of Arkansas for Medical sciences, Little Rock, AR, and the Università Campus Bio-Medico of Rome, Italy.

Whole-Exome Sequencing and Analysis. Genomic DNA from 66 tumor samples including two mixed NETc samples containing both neuroendocrine and adenocarcinoma cells were sent for WES. The sequencing data were processed using the GATK Best Practice workflow (36–38). After determining tumor purity, somatic SNVs were called using GATK4 MuTect2 (39) and INDELs were called using the intersection of the two callers, MuTect2 and Strelka2 (40) for tumor-normal paired tissues, and for unmatched tumors, MuTect2 was used. Gene burden analysis was performed using Mutpanning (41). Mutational matrices were constructed using SigProfilerMatrixGenerator (42), and mutational signatures were extracted per Alexandrov's et al. (11). Variants in genes implicated in the pathogenesis of NETc were verified by direct Sanger sequencing in the available samples. See also *SI Appendix, Materials and Methods* for details.

Somatic CNV Analysis. Somatic CNVs were primarily called from 57 paired samples with WES using FACETS (43), with CNVkit (44) and EXCAVATOR (45) used

as alternatives to improve specificity while enrichment analysis was performed using GISTIC2.0 (46) (see *SI Appendix, Materials and Methods* for details).

Transcriptome Sequencing and Gene Fusion Analysis. Eight NETc samples were subjected to RNA-Seq. Sequencing reads were aligned and processed using HISAT2 (47) and HTSeq-count (48). Gene differential expression was analyzed using DESeq2 (49) while gene fusion events were identified using Arriba (50). Gene fusions with medium to high confidence or previously reported in Arriba were considered.

HPV Detection and Integration Analysis. HPVDetector v.1.0 (51) was used to quantify HPV in WES data for the 143 types of HPV from the Papillomavirus Episteme (PaVE). There are two options in HPVDetector, QuickDetect to identify the presence of HPV types and Integration mode to determine the genomic location for the site of integration. We determined true HPV infection using QuickDetect mode.

Clonality Analysis. To infer clonal population structures in cancers, PyClone utilized a Bayesian clustering method to categorize sets of somatic mutations into potential clonal clusters, while also estimating their cellular prevalence and taking into consideration allelic imbalances resulting from segmental copy number alterations and normal-cell contamination (25). Reconstruction of clonal evolution was done using ClonEvol, which offers a comprehensive solution for clonal ordering, visualization, and interpretation (26).

Xenograft Implantation and In Vivo Drug Study. Briefly, the NET19 and NET21 PDX were xenografted in female CB17/lcrHsd-Prkd/scid mice subcutaneously into the lower abdomen area as previously described (52). Dosing began upon reaching target size and was delivered intravenously daily for copanlisib and orally BID for afatinib and elimusertib as either single agents or in combinations (see *SI Appendix, Materials and Methods* for details). After the last dose administration, animals were either euthanized per Yale Institutional Animal Care and Use Committe guidelines or followed for survival. All mice were housed and treated in accordance with the policies set forth by the Institutional Animal Care and Use Committee (IACUC) at Yale University.

Data, Materials, and Software Availability. All data discussed in the paper are available in Dataset S1.

Author affiliations: [a]Department of Obstetrics, Gynecology and Reproductive Sciences, Yale University School of Medicine, New Haven, CT 06510; [b]Department of Biomedical Sciences, Korea University College of Medicine, Seoul 02841, Korea; [c]Centre for Cancer Biomarkers, Department of Clinical Science, University of Bergen, Bergen 5021, Norway; [d]Department of Obstetrics and Gynecology, Haukeland University Hospital, Bergen 5009, Norway; [e]Department of Pathology, Yale University School of Medicine, New Haven, CT 06510; [f]First Pathology Division, Fondazione Istituti di Ricovero e Cura a Carattere Scientifico (IRCCS) Istituto Nazionale dei Tumori di Milano, Milano 20133, Italy; [g]Unit of Gynecologic Oncology, Department Woman and Child Health Sciences and Public Health, Fondazione Policlinico Universitario A. Gemelli Istituti di Ricovero e Cura a Carattere Scientifico (IRCCS), Rome 00168, Italy; [h]"Angelo Nocivelli" Institute of Molecular Medicine, Department of Obstetrics and Gynecology, Azienda Socio Sanitaria Territoriale (ASST) Spedali Civili and University of Brescia, Brescia 25123, Italy; [i]Department of Pathology, University of Arkansas for Medical Sciences, Little Rock, AR 72205; [j]Department of Obstetrics and Gynecology, Università Campus Bio-Medico di Roma, Rome 00128, Italy; [k]Department of Genitourinary Oncology, Human Oncology and Pathogenesis Program, Memorial Sloan Kettering Cancer Center, New York, NY 10069; [l]Department of Cellular and Molecular Medicine, University of California San Diego, San Diego, CA 92093; [m]Department of Biostatistics, University of Arkansas for Medical Sciences, Little Rock, AR 72205; and [n]Department of Pharmacology, Yale University School of Medicine, New Haven, CT 06520

Author contributions: S.B., K.J., J.S., and A.D.S. designed research; M.K.H., C.K., B.M., M.G., L.M., C.D., T.M.P.H., Y.Y.-H., N.B., P.H., and E.B. performed research; M.Z., F.R., S.L., B.P., M.M., E.P., G.S., G.A., A.R., G.S.H., V.A., M.C., E.R., M.A., P.E.S., C.M.Q., R.A., C.T., and J.S. contributed new reagents/analytic tools; S.Z., S.N., L.B.A., and E.R.S. analyzed data; and J.C. and A.D.S. wrote the paper.

Reviewers: O.D., Stanford University; and G.E.K., David Geffen School of Medicine at University of California Los Angeles.

Competing interest statement: A.D.S. is listed as author in a paper (i.e., *N. Engl. J. Med.* 2022; 386:437–448, DOI: 10.1056/NEJMoa2108330) where G.E.K. is listed as group author. A.D.S. had no interactions with G.E.K. (or any other of the 309-KEYNOTE-775 multicenter clinical trial Investigators) over the course of the research and writing of this paper.

1. A. Gadducci, S. Carinelli, G. Aletti, Neuroendrocrine tumors of the uterine cervix: A therapeutic challenge for gynecologic oncologists. *Gynecol. Oncol.* **144**, 637–646 (2017).
2. B. E. Howitt, P. Kelly, W. Glenn McCluggage, Pathology of neuroendocrine tumours of the female genital tract. *Curr. Oncol. Rep.* **19**, 59 (2017), 10.1007/s11912-017-0617-2.
3. M. E. McCusker, T. R. Coté, L. X. Clegg, F. J. Tavassoli, Endocrine tumors of the uterine cervix: Incidence, demographics, and survival with comparison to squamous cell carcinoma. *Gynecol. Oncol.* **88**, 333–339 (2003).
4. X. Pei *et al.*, The next generation sequencing of cancer-related genes in small cell neuroendocrine carcinoma of the cervix. *Gynecol. Oncol.* **161**, 779–786 (2021).
5. R. T. Hillman *et al.*, Comparative genomics of high grade neuroendocrine carcinoma of the cervix. *PLoS One* **15**, e0234505 (2020), 10.1371/journal.pone.0234505.
6. R. N. Eskander *et al.*, Unique genomic landscape of high-grade neuroendocrine cervical carcinoma: Implications for rethinking current treatment paradigms. *JCO Precis. Oncol.* **4**, (2020), 10.1200/po.19.00248.
7. A. M. Schultheis *et al.*, Genomic characterization of small cell carcinomas of the uterine cervix. *Mol. Oncol.* **16**, 833–845 (2022).
8. S. Y. Cho *et al.*, Cervical small cell neuroendocrine tumor mutation profiles via whole exome sequencing. *Oncotarget* **8**, 8095–8104 (2017).
9. L. Zammataro *et al.*, Whole-exome sequencing of cervical carcinomas identifies activating ERBB2 and PIK3CA mutations as targets for combination therapy. *Proc. Natl. Acad. Sci. U.S.A.* **116**, 22730–22736 (2019).
10. R. D. Burk *et al.*, Integrated genomic and molecular characterization of cervical cancer. *Nature* **543**, 378–384 (2017).
11. L. B. Alexandrov *et al.*, The repertoire of mutational signatures in human cancer. *Nature* **578**, 94–101 (2020).
12. C. Palles *et al.*, Germline MBD4 deficiency causes a multi-tumor predisposition syndrome. *Am. J. Hum. Genet.* **109**, 953–960 (2022).
13. P. A. Johansson *et al.*, Prolonged stable disease in a uveal melanoma patient with germline MBD4 nonsense mutation treated with pembrolizumab and ipilimumab. *Immunogenetics* **71**, 433–436 (2019).
14. M. Rodrigues *et al.*, Outlier response to anti-PD1 in uveal melanoma reveals germline MBD4 mutations in hypermutated tumors. *Nat. Commun.* **9**, 1866 (2018), 10.1038/s41467-018-04322-5.
15. S. O. Sulima *et al.*, Ribosomal lesions promote oncogenic mutagenesis. *Cancer Res.* **79**, 320–327 (2019).
16. M. Avissar-Whiting *et al.*, Polycomb group genes are targets of aberrant DNA methylation in renal cell carcinoma. *Epigenetics* **6**, 703–709 (2011).
17. J. S. Crabtree, C. S. Singleton, L. Miele, Notch signaling in neuroendocrine tumors. *Front. Oncol.* **6**, 94 (2016), 10.3389/fonc.2016.00094.
18. P. Mittal, C. W. M. Roberts, The SWI/SNF complex in cancer – biology, biomarkers and therapy. *Nat. Rev. Clin. Oncol.* **17**, 435–448 (2020).
19. T. Sasahira *et al.*, A comprehensive expression analysis of the MIA gene family in malignancies: MIA gene family members are novel, useful markers of esophageal, lung, and cervical squamous cell carcinoma. *Oncotarget* **7**, 31137–31152 (2016).
20. P. Filimonenko *et al.*, The selective macroautophagic degradation of aggregated proteins requires the Pi3P-binding protein Alfy. *Mol. Cell* **38**, 265–279 (2010).
21. R. K. Amaravadi, A. C. Kimmelman, J. Debnath, Targeting autophagy in cancer: Recent advances and future directions. *Cancer Discov.* **9**, 1167–1181 (2019).
22. B. S. Simpson *et al.*, Genetic alterations in the 3q26.31-32 locus confer an aggressive prostate cancer phenotype. *Commun. Biol.* **3**, 440 (2020), 10.1038/s42003-020-01175-x.
23. K. W. Huang *et al.*, MTL-CEBPA combined with immunotherapy or RFA enhances immunological anti-tumor response in preclinical models. *Int. J. Mol. Sci.* **22**, 9168 (2021).
24. R. Kanteti *et al.*, PAX5 is expressed in small-cell lung cancer and positively regulates c-Met transcription. *Lab. Invest.* **89**, 301–314 (2009).
25. A. Roth *et al.*, PyClone: Statistical inference of clonal population structure in cancer. *Nat. Methods* **11**, 396–398 (2014).
26. H. X. Dang *et al.*, ClonEvol: Clonal ordering and visualization in cancer sequencing. *Ann. Oncol.* **28**, 3076–3082 (2017).
27. A. Bellacosa *et al.*, MED1, a novel human methyl-CpG-binding endonuclease, interacts with DNA mismatch repair protein MLH1. *Proc. Natl. Acad. Sci. U.S.A.* **96**, 3969–3974 (1999).
28. S. E. Paraghamian, T. C. Longoria, R. N. Eskander, Metastatic small cell neuroendocrine carcinoma of the cervix treated with the PD-1 inhibitor, nivolumab: A case report. *Gynecol. Oncol. Res. Practice* **4**, 3 (2017), 10.1186/s40661-017-0038-9.
29. A. Sharabi *et al.*, Exceptional response to nivolumab and stereotactic body radiation therapy (SBRT) in neuroendocrine cervical carcinoma with high tumor mutational burden: Management considerations from the center for personalized cancer therapy at UC San Diego moores cancer center. *Oncologist* **22**, 631–637 (2017).
30. E. Bonazzoli *et al.*, Inhibition of BET bromodomain proteins with GS-5829 and GS-626510 in uterine serous carcinoma, a biologically aggressive variant of endometrial cancer. *Clin. Cancer Res.* **24**, 4845–4853 (2018).
31. E. Cocco *et al.*, Dual CCNE1/PIK3CA targeting is synergistic in CCNE1-Amplified/PIK3CA-mutated uterine serous carcinomas in vitro and in vivo. *Br. J. Cancer* **115**, 303–311 (2016).
32. X. Duan *et al.*, MR imaging features and staging of neuroendocrine carcinomas of the uterine cervix with pathological correlations. *European Radiol.* **26**, 4293–4302 (2016).
33. A. B. Hanker, V. Kaklamani, C. L. Arteaga, Challenges for the clinical development of PI3K inhibitors: Strategies to improve their impact in solid tumors. *Cancer Discov.* **9**, 482–491 (2019).
34. M. A. Earp *et al.*, Characterization of fusion genes in common and rare epithelial ovarian cancer histologic subtypes. *Oncotarget* **8**, 46891–46899 (2017).
35. K. Jin *et al.*, Long non-coding RNA PVT1 interacts with MYC and its downstream molecules to synergistically promote tumorigenesis. *Cell. Mol. Life Sci.* **76**, 4275–4289 (2019).
36. A. McKenna *et al.*, The genome analysis toolkit: A MapReduce framework for analyzing next-generation DNA sequencing data. *Genome Res.* **20**, 1297–1303 (2010).
37. G. A. Van der Auwera *et al.*, From fastQ data to high-confidence variant calls: The genome analysis toolkit best practices pipeline. *Curr. Protoc. Bioinform.* **11**, 11.10.1–11.10.33 (2013), 10.1002/0471250953.bi1110s43.
38. 1000 Genomes Project Consortium *et al.*, A global reference for human genetic variation. *Nature* **526**, 68–74 (2015).
39. D. Benjamin *et al.*, Calling somatic SNVs and indels with Mutect2. bioRxiv [Preprint] (2019). https://doi.org/10.1101/861054 (Accessed 12 February 2019).
40. S. Kim *et al.*, Strelka2: Fast and accurate calling of germline and somatic variants. *Nat. Methods* **15**, 591–594 (2018).
41. M. S. Lawrence *et al.*, Mutational heterogeneity in cancer and the search for new cancer-associated genes. *Nature* **499**, 214–218 (2013).
42. E. N. Bergstrom *et al.*, SigProfilerMatrixGenerator: A tool for visualizing and exploring patterns of small mutational events. *BMC Genomics* **20**, 685 (2019), 10.1186/s12864-019-6041-2.
43. R. Shen, V. E. Seshan, FACETS: Allele-specific copy number and clonal heterogeneity analysis tool for high-throughput DNA sequencing. *Nucleic Acids Res.* **44**, e131 (2016), 10.1093/nar/gkw520.
44. E. Talevich, A. H. Shain, T. Botton, B. C. Bastian, CNVkit: Genome-wide copy number detection and visualization from targeted DNA sequencing. *PLoS Comput. Biol.* **12**, e1004873 (2016), 10.1371/journal.pcbi.1004873.
45. A. Magi *et al.*, EXCAVATOR: Detecting copy number variants from whole-exome sequencing data. *Genome Biol.* **14**, R120 (2013), 10.1186/gb-2013-14-10-r120.
46. C. H. Mermel *et al.*, GISTIC2.0 facilitates sensitive and confident localization of the targets of focal somatic copy-number alteration in human cancers. *Genome Biol.* **12**, R41 (2011), 10.1186/gb-2011-12-4-r41.
47. M. Pertea, D. Kim, G. M. Pertea, J. T. Leek, S. L. Salzberg, Transcript-level expression analysis of RNA-seq experiments with HISAT, StringTie and Ballgown. *Nat. Protocols* **11**, 1650–1667 (2016).
48. S. Anders, P. T. Pyl, W. Huber, HTSeq-A Python framework to work with high-throughput sequencing data. *Bioinformatics* **31**, 166–169 (2015).
49. M. I. Love, W. Huber, S. Anders, Moderated estimation of fold change and dispersion for RNA-seq data with DESeq2. *Genome Biol.* **15**, 550 (2014), 10.1186/s13059-014-0550-8.
50. S. Uhrig *et al.*, Accurate and efficient detection of gene fusions from RNA sequencing data. *Genome Res.* **31**, 448–460 (2021).
51. P. Chandrani *et al.*, NGS-based approach to determine the presence of HPV and their sites of integration in human cancer genome. *Br. J. Cancer* **112**, 1958–1965 (2015).
52. S. Zhao *et al.*, Mutational landscape of uterine and ovarian carcinosarcomas implicates histone genes in epithelial–mesenchymal transition. *Proc. Natl. Acad. Sci. U.S.A.* **113**, 12238–12243 (2016).